Article

Potentiating the anti-cancer properties of bisphosphonates by nanocomplexation with the cationic amphipathic peptide, RALA.

Ashley S. Massey, Sreekanth Pentlavalli, Richard Cunningham, Cian M McCrudden, Emma M McErlean, Philip Redpath, Ahlam A Ali, Stephanie Annett, John W McBride, Joanne McCaffrey, Tracy Robson, Marie Eugenie Migaud, and Helen O. McCarthy

Mol. Pharmaceutics, **Just Accepted Manuscript** • DOI: 10.1021/acs.molpharmaceut.5b00670 • Publication Date (Web): 08 Mar 2016

Potentiating the anti-cancer properties of bisphosphonates by nanocomplexation with the cationic amphipathic peptide, RALA.

Ashley S. Massey, PhD, Sreekanth Pentlavalli, PhD, Richard Cunningham, PhD, Cian M. McCrudden, PhD, Emma M. McErlean, Philip Redpath, PhD, Ahlam A. Ali, PhD, Stephanie Annett, John McBride, PhD, Joanne McCaffrey, PhD, Tracy Robson, PhD, Marie E. Migaud, PhD, Helen O. McCarthy, PhD*

School of Pharmacy, Queen's University Belfast, 97 Lisburn Road, Belfast, Northern Ireland, BT9 7BL

Corresponding author: Helen O. McCarthy; h.mccarthy@qub.ac.uk; 02890972149

Abstract

Bisphosphonates (BPs) are a class of bone resorptive drug with a high affinity for the hydroxyapatite structure of bone matrices that are used for the treatment of osteoporosis. However, clinical application is limited by a common toxicity, BP-related osteonecrosis of the jaw. There is emerging evidence that BPs possess anti-cancer potential, but exploitation of these anti-proliferative properties is limited by their toxicities. We previously reported the utility of a cationic amphipathic fusogenic peptide, RALA, to traffic anionic nucleic acids into various cell types in the form of cationic nanoparticles. We hypothesized that complexation with RALA could similarly be used to conceal a BP's hydroxyapatite affinity, and to enhance bioavailability, and thereby enhancing anti-cancer efficacy.

Incubation of RALA with alendronate, etidronate, risedronate or zoledronate provoked spontaneous electrostatic formation of cationic nanoparticles that did not

exceed 100 nm in diameter, and that were stable over a range of temperatures and for up to 6 h. The nanoparticles demonstrated a pH responsiveness, possibly indicative of a conformational change, that could facilitate release of the BP cargo in the endosomal environment. RALA/BP nanoparticles were more potent anti-cancer agents than their free BP counterparts in assays investigating the viability of PC3 prostate cancer and MDA-MB-231 breast cancer cells. Moreover, RALA complexation potentiated the tumour growth delay activity of alendronate in a PC3 xenograft model of prostate cancer. Taken together, these findings further validate the use of BPs as repurposed anti-cancer agents.

Key words: Alendronate; Prostate cancer; Bisphosphonates; Cell penetrating peptides; Self-assembling nanoparticles

Introduction

Over the past two decades, bisphosphonates (BPs) have become mainstream therapeutics in the treatment of diseases with excessive bone turnover[1]. The pharmacological properties of BPs are dictated by their distinct mechanism of action; binding to the calcium-containing bone matrix, release from the matrix by osteoclasts and intracellular localisation during the bone remodelling process. Etidronate is one of the first generation BPs, characterised by a short side-chain (Fig. 1A), which destabilises osteoclast homeostasis via conversion into an ATP like molecule, which in turn acts as an inhibitor to a number of ATP-dependent enzymes and processes.

The second and third generation of anti-osteoclastic BPs are nitrogen-containing BPs (N-BPs; e.g. alendronate, risedronate and zoledronate; Fig. 1A), potent inhibitors of farnesyl pyrophosphate synthase, and significantly more effective than the first generation BPs in reducing bone remodelling. The anti-osteoclastic activity, mode of action and selective biodistribution has enabled N-BPs to be utilised as palliative agents for metastatic bone disease, particularly for breast and prostate cancer[2]. In such cancers, where bone metastases are common, the N-BPs reduce bone resorption and in turn alleviate skeletal related events such as fractures and bone pain. More recently, however the adjuvant use of BPs with cytotoxic agents has highlighted their synergistic effects, beyond basic anti-resorptive activities. Indeed N-BPs exhibit a range of anti-tumour effects *in vitro,* including inhibition of tumour growth[3], migration, invasion, adhesion and angiogenesis[4-6], with synergistic effects dependent on side chain structure[7]. Furthermore, a number of clinical trials

involving more than 20,000 patients observed the positive effects of co-administration of BPs with hormonal therapies and chemotherapeutics on the occurrence of bone metastases and recurrence of disease[8].

However, despite more than a decade of research into understanding the molecular mechanisms of the anti-tumour effects of the BPs, to date the only successful *in vivo* applications have been in the prevention of bone metastases[9]. It is postulated that the change in the bone microenvironment stemming from the BPs leads to the positive synergistic pharmacological outcomes, thus supporting the 'seed and soil' theory[10]. There are two factors that limit the translation of *in vitro* effects to anti-tumour effects *in vivo*. Firstly, the presence of a hydroxyl and two phosphonate groups flanking a carbon atom confers high affinity for the bone matrix and so the initially circulating BP is not excreted by the kidneys. Secondly, the concentration of circulating BP required to exert the desired anti-tumour effects is so high that adverse side-effects will ensue[11].

BPs have potential as anti-tumour agents for soft tissue tumours outside the bone environment. Liposomes have been employed as delivery systems for BPs to increase circulation times and exploit the anti-tumour effect; liposomal encapsulation of neridronate increased its cytotoxicity in MDA-MB-231 breast cancer cells (EC_{50} of 95 μM, compared to 1.7 μM)[12]. Furthermore, it inhibited migration and invasion significantly more than the free drug and at a lower concentration, and caused a significant reduction in MMP-2 and MMP-9 expression[12]. Marra *et al* advanced the liposome model by assessing PEGylated liposomes for the delivery of zoledronate in both an *in vitro* and *in vivo* setting[13].

Upon encapsulation, potentiation factors of greater than one were achieved in all cell lines assessed, indicating a strong enhancement of tumour cell growth inhibition[13]. Intravenous delivery of zoledronate in PEGylated liposomes to a PC3 prostate cancer xenograft model *in vivo* significantly improved overall survival when compared to free zoledronate-treated mice[13]. Anti-tumour effects were further enhanced when calcium phosphate was used to aid delivery by complexing zoledronate into nanoparticles prior to encapsulation with PEGylated liposomes[14].

In this study we utilised a peptide delivery system (RALA) to investigate for the first time the impact of a fusogenic amphipathic peptide on the bioavailability and potency of BPs, and in particular, alendronate. RALA is an arginine-rich amphipathic peptide which has shown potential to efficiently deliver nucleic acids *in vitro* and *in vivo*[15]. RALA consists of a hydrophobic and hydrophilic region, which facilitates interaction with the lipid bilayers, thus enabling transport of nucleic acids across cellular membranes. In addition the lower pH in the endosome alters the alpha-helical conformation of RALA, which enables endosomal disruption and release of the cargo into the cytosol. We hypothesised that RALA would condense the BP class of drugs into nano-sized particles, which would significantly improve the potency, anti-tumour effects and confer significant repurposing potential.

Experimental

Analytical TLC was performed with Merck Silica gel 60 F_{254} plates. Visualisation was accomplished by UV-light (λ = 254 nm) and/or staining with an anisaldehyde or potassium permanganate solution, followed by heating. ^{1}H, ^{13}C and 2D (H-COSY, HMQC) NMR spectra were all recorded on Brüker avance DPX 400. The chemical shifts (δ) are reported in ppm (parts per million). High-resolution mass spectrometry (HRMS) was recorded on a VG Quattro Triple Quadropole Mass Spectrometer (ES). pH measurements were performed using a HANNA HI 2211 pH meter.

Synthesis of the BP

All BPs were used in their acidic forms. Risedronic acid[16] and zoledronic acid[17-19] were synthesised in house using literature procedure while alendronate and etidronate were obtained from Aroz Technologies (Cincinnati, Ohio, USA). All other reagents were purchased from Sigma Aldrich and used as supplied without any further purification.

Synthesis of Risedronic acid:

To 3-pyridyl acetic acid hydrochloride (2.0 g, 11.5 mmol, 1.0 eq), in a 100 mL two necked flask equipped with a reflux condenser, was added neat phosphorous acid (3.6 g, 43.8 mmol, 3.8 eq) and p-nitrophenol (12.0 g, 86.3 mmol, 7.5 eq). The mixture was heated to 90 °C for 2 h until all of the solid had melted, forming a thick suspension. Phosphorous trichloride (7.0 g, 50.0 mmol, 4.3 eq) was added to this suspension, kept at 90 °C for 6 h, after which a yellow, gel-like material was formed. After cooling to room temperature (19°C), water (20 mL) was added and the

mixture was left at reflux for 12 h. Methanol (15 mL) was then added, and the precipitated product was kept stirring at 0 ° C for 2 h. The white, amorphous product obtained was filtered under vacuum using Whatman filter paper and washed with methanol (100 mL) to yield 3.3 g (80 %) of the titled compound. ^{1}H NMR (D_2O, 400 MHz): δ ppm 3.37 (2H, t, J_{HP} = 12.1 Hz, C$\underline{H}_2$Pyr), 7.81-7.87 (1H, m, Pyr), 8.50 (2H, t, J = 6.0 Hz, Pyr), 8.65 (1H, s, Pyr); ^{13}C NMR (D_2O, 125 MHz): δ ppm: 37.0 ($\underline{C}H_2$Pyr), 73.1-75.7 (t, J_{CP} = 128.3 Hz. PCP), 126.8 (Pyr), 138.8 (Pyr), 139.5 (Pyr), 143.3 (Pyr), 149.8 (Pyr); ^{31}P-NMR (D_2O, 162 MHz): δ ppm: 16.6; HRMS (ES+ , m/z) calcd for $(M+H)^+$ $C_7H_{12}O_7P_2$: 284.0089; found: 284.0082

Synthesis of imidazol-1-yl-acetic acid hydrochloride:

To a solution of imidazole (0.5 g, 7.4 mmol, 1.0 eq) and Cs_2CO_3 (2.9 g, 8.8 mmol, 1.2 eq) in dry dimethylformamide (30 mL) was added ethyl bromoacetate (0.9 mL, 8.1 mmol, 1.1 eq) at RT and stirred for 24 h. The inorganic salts were filtered off, and the filtrate was concentrated. The residue was then taken up in dichloromethane (40 mL) and washed with H_2O (2 x 50 mL). The organic phase was dried over ($MgSO_4$), filtered through Whatman filter paper, and concentrated to afford ethyl-1*H*-imidazole-1-acetate. The crude ester intermediate was solubilised in dioxane/6M HCl (1:1, 20 mL), refluxed for 4 h. After removal of the volatiles under reduced pressure, the crude imidazol-1-yl acetic acid was obtained as an orange solid deemed pure enough by NMR for the subsequent step, 0.8 g (91 %) yield. ^{1}H NMR (D_2O, 400 MHz): δ 4.97 (2H, s, C$\underline{H}_2$COOH), 7.33–7.36 (m, 2H, NC$\underline{H}$C$\underline{H}$N), 8.63 (s, 1H, NC$\underline{H}$N); ^{13}C NMR (D_2O, 125 MHz): δ ppm: 49.9 ($\underline{C}H_2$COOH), 119.6, 123.1 (N$\underline{C}$H$\underline{C}$HN), 136.0 (N$\underline{C}$HN), 170.2 ($\underline{C}$OOH).

Synthesis of Zoledronic acid:

To a suspension of imidazol-1-yl-acetic acid hydrochloride (1.0 g, 8.0 mmol, 1.0 eq) and phosphorous acid (2.0 g, 23.0 mmol, 3.0 eq) in chlorobenzene (10 mL) was added phosphorous oxychloride (2.2 mL, 23.0 mmol, 3.0 eq) at 85 ^{o}C for 2 h then heated to 95 °C for 2.5 h. The reaction mixture was cooled to 60 ^{o}C and water (20 mL) was added. The aqueous layer was separated, collected and refluxed for 18 h. It was cooled to 19°C and diluted with methanol (20 mL). The mixture was cooled to 0-5 ^{o}C and stirred for 3 h. The precipitated solid was filtered, washed with cold water (100 mL) followed by methanol (100 mL) and dried under vacuum at 60 ^{o}C for 12 h to afford the zoledronic acid (isolated yield 1.3 g (64 %) as a white solid. ^{1}H NMR (D_2O, 400 MHz): δ ppm: 4.61 (2H, t, J_{HP} = 9.2 Hz, C$\underline{H}_2$Ar), 7.29 (1H, s, NC$\underline{H}$), 7.44 (1H, s, NC$\underline{H}$), 8.63 (1H, s, NC$\underline{H}$N); ^{13}C NMR (D_2O, 125 MHz): δ ppm: 53.4 ($\underline{C}H_2$Ar), 72.8 (t, J_{CP} = 135.7 Hz, P$\underline{C}$P), 119.1 (N$\underline{C}$H), 124.7 (N$\underline{C}$H), 136.7 (N$\underline{C}$HN); ^{31}P-NMR (D_2O, 162 MHz): δ ppm 13.9, HRMS (ES+ , m/z) calcd for $(M+H)^+$ $C_5H_9O_7P_2$: 270.9887; found: 270.9885.

Preparation of RALA peptide

RALA peptide was produced as an acetate salt by solid-state synthesis (FMOC chemistry) (Biomatik, UK) and was reconstituted in molecular grade water (Invitrogen, UK) such that a final concentration of 5.8 mg/ml was achieved. Reconstituted peptide was stored in aliquots at -20°C.

Preparation of BPs

Each BP was reconstituted in molecular grade water to give a concentration of 10 mM. A serial dilution was carried out such that a 1 mM working concentration was

achieved. The reconstituted BPs were stored at 19°C (room temperature) for further use.

Formulation of RALA/BP nanoparticles

Each BP was complexed with the fusogenic peptide RALA according to a mass ratio of peptide to BP. For example to achieve a ratio of 10:1, 10 µg of RALA was added to 1 µg of BP in aqueous solution. Samples were allowed to incubate at 19°C for approximately 30 min before physicochemical characterisation of the nanoparticles. Nanoparticles were complexed in UltraPure™ DNase/RNase-Free Distilled Water (Invitrogen), pH 7.0.

Particle size analysis

The mean hydrodynamic particle size measurements for RALA/BP complexes were performed using Dynamic Light Scattering (DLS) by a Malvern Zetasizer Nano ZS instrument with DTS software. After incubation of complexes at 19°C for 30 min, mean size by number was measured at 20°C.

Zeta potential analysis

Zeta potential measurements of RALA/BP complexes were determined by Laser Doppler Velocimetry using the Malvern Zetasizer Nano ZS instrument and DTS software (Malvern Instruments, UK). Nanoparticle size and charge were compared using one-way ANOVA with Dunnett's multiple comparison test using particle size at mass ratio 10 as comparator. (Mass ratio 10 was used as a comparator, as this was the lowest mass ratio at which there was excellent agreement between BPs in terms of particle size and charge across the range of BPs; mass ratio 10 was used for

subsequent *in vitro* and *in vivo* experiments for this reason; (for comparative figure, see Supplementary Figure 1).

Temperature study

RALA/BP nanoparticles were formed at a mass ratio of 10:1 and allowed to incubate at 19°C for 30 min. Malvern Zetasizer Nano ZS with DTS software was used to measure the mean hydrodynamic size of the complexes over a temperature range of 4-37°C at 3°C intervals. Nanoparticle sizes were compared using one-way ANOVA with Dunnett's multiple comparison test; sizes were analyzed using 4°C, 19°C and 37°C as comparators (cold storage, room temperature and body temperature).

Incubation study

For assessment of the physical stability of the nanoparticles over a period of time, RALA/BP nanoparticles were prepared at a mass ratio of 10:1 and the mean hydrodynamic size was measured using Malvern Zetasizer Nano ZS with DTS software at 30 min intervals starting immediately after particles are prepared and continuing for 6 h (samples were held at 20°C between intervals). Nanoparticle sizes were compared using one-way ANOVA with Dunnett's multiple comparison test using particle size at 0 min as comparator.

Transmission electron microscopy

RALA/BP nanoparticles were prepared at a mass ratio of 10:1 and loaded onto carbon reinforced, formvar coated, 200 mesh copper grids (Agar Scientific, UK). After drying, the grids were stained with 5% aqueous uranyl acetate for 5 min at 19°C. The nanoparticles were imaged using a JEOL 100CXII transmission electron

microscope at an accelerating voltage of 80 kV and images were captured onto Kodak 4489 Electron Microscope Film.

Cell culture and maintenance

PC3 prostate cancer cells and MDA-MB-231 breast cancer cells (ATCC, Manassas, VA) were maintained as monolayers in RPMI 1640 medium (Invitrogen, UK) and Dulbecco's modified Eagle's medium (DMEM) (Invitrogen, UK) respectively supplemented with 10% foetal calf serum (PAA, UK). Cells were maintained in an incubator at 37°C with 5% CO_2 atmosphere. All *in vitro* cell experiments were carried out at 37°C in a 5% CO_2 incubator. Cultures were routinely assessed for mycoplasma contamination using Plasmotest reagents (Invivogen, France).

Nanoparticle internalization

Alendronate and zoledronate were complexed (at mass ratio 10) into nanoparticles using fluorescein isothiocyanate (FITC)-conjugated RALA in the same manner as described previously. The impact of FITC on the size and charge of nanoparticles was assessed using Student's unpaired *t*-test. PC3s and MDA-MB-231s plated at 50,000 cells per well of 24 well plates were exposed to FITC-RALA/BP nanoparticles, or free FITC-RALA alone for up to 2 h. Excess extracellular nanoparticles were removed by washing with PBS, and cells were trypsinized and resuspended in PBS. The proportion of cells positive for FITC was assessed using a BD FACScalibur flow cytometer.

In an attempt to demonstrate nanoparticle internalization, PC3s and MDA-MB-231s grown on glass coverslips (Thermo Scientific, UK) were treated with FITC-RALA/BP nanoparticles, or free FITC-RALA for 1 h, following which they were fixed and

mounted onto microscope slides with ProLong® Diamond Antifade Mountant with DAPI (Life Technologies, UK). Cells were viewed using a Leica SP5 confocal fluorescence microscope, and analysis was performed using LAS AF Lite software (Leica). Orthogonal sectioning was performed to determine the cellular localization of FITC-conjugated particles.

Cell viability

Cell viability was evaluated by both MTS assay with CellTiter 96 Aqueous One Solution Cell Proliferation Assay (Promega, UK) and manual counting of the viable adherent cells using a haemocytometer with Trypan Blue exclusion staining. PC3 prostate cancer cells and MDA-MB-231 breast cancer cells were seeded at a density of 1 x 10^4 cells per well and allowed to adhere. Cells were conditioned in OptiMEM serum-free medium (Invitrogen, UK) for 2 h prior to treatment with solutions of BP to achieve a final exposure concentration of 5 µM to 2 mM. RALA/BP nanoparticles were prepared using a mass ratio of 10:1, such that the final concentration of BP per well was in the range 5 µM to 250 µM. To investigate the impact of RALA carrying a non-toxic cargo, RALA/pEGFP-N1 nanoparticles (which share physicochemical properties of the RALA/BP particles) were used to treat PC3s, such that the amount of RALA in each well was equivalent to that found in wells treated with RALA/alendronate (and approximated the amounts in the other RALA/BP wells). Cells were incubated for 6 h following treatment before medium was replaced with complete culture medium and the cells incubated for a further 72 h.

For the MTS assay, treatment was as above. CellTitre reagent was added to each well to a final concentration of 10%, and plates were returned to the incubator for 2

h. Absorbance was read at 490 nm using a Bio-Tek Powerwave XS plate reader with Gen5 software, and any background absorbance was subtracted from readings. Cell viability was expressed as a percentage of that of the untreated control. Data (for which dose-response relationships were evident) were normalized using GraphPad Prism version 6.0g for OS-X (using the equation Y=100/(1+10^((X-LogEC50))) to recalculate Y values). Non-linear regression analysis was used to fit sigmoidal dose-response curves to the data, and EC_{50}s for the different conditions were calculated.

***In vivo* xenograft model**

All protocols conform to the UK Scientific Act of 1986 and were performed under the project license 2678. The male BALB-C SCID mice were anaesthetised using 4% isofluorane (Abbott, UK) and injected intradermally on the rear dorsum with 5 x 10^6 PC3 cells. When the tumour volume reached approximately 100 mm^3 the mice were randomised and divided into 4 groups (n=3/group) and treated with 10 µg alendronate only, RALA only, RALA/alendronate nanoparticles containing 10 µg alendronate, or received no treatment. Treatments were thrice weekly for three weeks, and were by intratumoural injection using a total volume of 100 µl. Digital calipers were used to measure the length (L), breadth (B) and depth (D) of the tumours; tumour volume was calculated using the formula -

$$V = \frac{4}{3}\boldsymbol{\pi} r^3$$

where r is half of the geometric mean diameter (GMD), calculated as –

$$\sqrt[3]{L*B*D}$$

For analysis of the *in vivo* results, ANOVA with Bonferroni *post hoc* test was used.

Immunohistochemistry

Once tumour volume had quadrupled, mice were sacrificed; tumours were removed and fixed in 10% formalin for 24 h, before embedding in paraffin wax and sectioning. Standard immunohistochemical procedures were used – xenograft Ki67 content was assessed using anti-Ki67 rabbit polyclonal antibody (ab833 – Abcam, UK), and horseradish peroxidase-conjugated anti-rabbit secondary antibody (Dako). Ki67 expression was visualised by addition of diaminobenzidine, and slides were counterstained in Harris hematoxylin. Whole specimen high-resolution images were captured, and viewed using PathXL.

Results

Synthesis and Characterisation of RALA/BP NPs

Each bisphosphonate (Fig. 1A) was complexed with the amphipathic peptide RALA (Fig. 1B) according to a mass ratio of peptide to BP.

RALA /BPs form spherical, nano-sized particles with a positive zeta potential

Characterisation of the RALA/BP nanoparticles confirmed the formation of nano-sized particles with a positive zeta potential (Fig. 1C-F). This was confirmed by TEM (Fig. 2). Both the size and charge of the NPs are ideal for cellular entry[15]. RALA successfully condensed the three N-BPs alendronate, risedronate and zoledronate into sub-100 nm sized particles from a mass ratio of 2:1 (RALA/BP) onwards. That etidronate does not form nanoparticles (<100 nm) below mass ratio 4:1 was not unexpected; its overall larger negative charge at physiological pH means that additional RALA is required to achieve a similar degree of neutralization. We did not assess the impact of pH differential on size/zeta potential across the range of BPs tested; however, in previous studies, we did not observe any appreciable impact of pH on the zeta potential of RALA/nucleic acid nanoparticles (unpublished data), which have similar physicochemical properties to RALA/BP particles. Small differences in pH may exist in the BP solutions before complexation with RALA, but we do not anticipate that this impacts on the physicochemical properties of the resulting nanoparticles.

RALA/BP nanoparticles show thermal stability over a 6 h time period

Nanoparticles were formed at a mass ratio of 10:1 for all BPs (Fig. 1C-F) and the particle size was analysed over a range of temperatures from 4°C to 37°C at 3°C intervals (Fig. 3A). The significance of size differences was analysed using 4°C (cold storage), 19°C (room temperature) and 37°C (human body temperature) as comparators; with the exception of alendronate, when particle size was significantly larger at 25°C than at 37°C, temperature did not affect particle size in any of the four BPs in the conditions tested.

In addition, the RALA/BP NPs were evaluated over a 6 h period (the duration of cellular exposure in *in vitro* experiments). All RALA/BP NPs were less than 80 nm in diameter across temperature range and incubation time ($p>0.05$; Fig. 3B), with no aggregation observed which is encouraging for *in vivo* administration. For each BP, the mean particle count ranged between 100-300 kcps, indicative of particle formation and presence. The PDI was consistently between 0.4-0.6 for all BP nanoparticles.

RALA/BP nanoparticles show stability over 48 h and are pH responsive

Stability of RALA/BP nanoparticles

RALA/BP (10:1 ratio) were analysed using ^{31}P NMR with trimethyl phosphate as internal standard. All RALA/BP nanoparticles were stable over a period of one week at neutral pH (one-way ANOVA with Dunnett's multiple comparison test revealed no significant variation in phosphorous content between any time point and T_0 in any of the tested BPs (Fig. 4A)). Moreover, the stability of RALA/BP nanoparticles at the 10:1 ratio was not dependent on the nature of the BPs' side chains and the

associated differences in lipophilic and electrostatic properties that each functional group confers to the BP. This study establishes that RALA can form nanoparticles with any BP tested (first or second generation) with a relatively low mole to mole ratio.

Effect of pH on RALA/BP nanoparticles

NPs were suspended in three aqueous solutions adjusted at different pH as shown in Fig. 4B-E (pH was adjusted by dropwise addition of 0.1 M HCl or NaOH, as appropriate). As expected from experience with RALA, these particles were stable at pH 7 and 9, but particles disassociated at acidic pH[15]. At this pH, RALA increases its alpha-helicity, which is essential for disruption of the endosomal membrane to facilitate release of the cargo into the cytoplasm. Thus the ^{31}P NMRs of all RALA/BP particles at this pH indicate a complete loss of the phosphonate signal, indicating that each BP precipitates out of solution along with the RALA peptide.

FITC-RALA/BP nanoparticles are rapidly internalized by cancer cells *in vitro*

Incubation of FITC-RALA with alendronate or zoledronate resulted in formation of cationic nanoparticles, similar to particles formed using unconjugated RALA. Nanoparticles comprising FITC-RALA and alendronate were not significantly different from those comprising RALA and alendronate, while FITC-RALA/zoledronate particles were slightly larger and slightly more positively charged than their unconjugated RALA counterparts (Fig. 5A).

FITC was detectable in PC3s and MDA-MB-231s following 5 min treatment with alendronate/zoledronate complexed with FITC/RALA, and in cells treated with free FITC-RALA (Fig. 5B). FITC-RALA treatment produced a diffuse staining pattern in

both cell types, whereas cells treated with either FITC-RALA/BP complex displayed more focused cytoplasmic staining. Orthogonal sectioning indicated that FITC fluorescent signal was produced intracellularly, rather than extracellularly (Fig. 5C).

RALA/BP nanoparticles demonstrate anti-tumour activity *in vitro*

PC3 prostate cancer and MDA-MB-231 breast cancer cells were either treated with free BP or RALA/BP nanoparticles at a range of concentrations for 6 h and then incubated for 72 h before evaluating cell viability. Complexation with RALA potentiated the effects of alendronate, etidronate and risedronate, although was without effect in the case of zoledronate (Table 3 & Figs. 6 & 7); conversely, complexes formed of RALA and pEGFP-N1 did not negatively impact the viability of PC3 (Fig. 6A). Perhaps most striking is the anti-cancer effects observed when etidronate or risedronate, themselves devoid of activity, were delivered using RALA (Fig. 6A). Of the N-BPs, alendronate was most impressively potentiated by RALA, so was selected for *in vivo* studies. Unlike in PC3s, complexation of zoledronate with RALA slightly increased its potency in MDA-MB-231s; in MDA-MB-231s, alendronate's potency was enhanced to a similar degree by RALA complexation as it was in PC3s (Fig. 7). There was generally good agreement between EC_{50} values generated by the two toxicity/viability assays (Figs. 6 & 7).

RALA/alendronate nanoparticles exhibit anti-tumour activity *in vivo*

Treatment with RALA only had no significant effect on tumour growth (Fig. 8A; $p=0.0792$). In contrast, both alendronate- and RALA/alendronate-treated tumours exhibited a significant growth delay compared to untreated controls ($p<0.0001$ and $p=0.0004$ respectively). Furthermore, the time taken for tumour volume to

quadruple was also significantly longer in the RALA/alendronate treated mice, suggesting that potentiation of anti-cancer properties seen in *in vitro* assays translated into the *in vivo* setting ($p=0.0019$; Fig. 8B). The endpoint of the experiment was tumour quadrupling; median survival for the groups were 16 days (control), 14 days (RALA), 19 days (free alendronate) and 26 days (RALA/alendronate) (Fig. 8B). A significant increase in survival time of RALA/alendronate nanoparticle treated mice of 56.3% was seen when compared to the untreated control group ($p<0.001$). The survival time of this group was also significantly higher compared to the alendronate only treated group at 32% ($p<0.01$) (Fig. 8C). Ki67 expression staining of xenograft sections was suggestive of an impact of RALA/alendronate on the proliferative capacity of the PC3 cells *in vivo* – the intensity of Ki67 staining was considerably stronger in control, RALA and alendronate samples than in the RALA/alendronate samples (Fig. 8D); given that RALA/alendronate possessed anti-proliferative capacity *in vitro*, this finding is unsurprising.

Discussion

This study has demonstrated for the first time that a peptide delivery system, RALA, can condense four different BPs into positively charged nanoparticles that are less than 100 nm in diameter, induce a significant potentiation factor *in vitro* and significantly retard tumour growth *in vivo*.

Major differences in mole: mole ratio between RALA and BP did not prevent the production of nanoparticles by RALA. In fact, with the exception of etidronate, mass

ratios (RALA:BP) as low as 2:1 elicited the desired size; this corresponded to a mole to mole ratio of 0.40 (Table 2). The higher ratio of 4:1 observed for the RALA:etidronate nanoparticles can be explained by the lack of a charged polar functional group. Here, while one could see the amino or aromatic amino groups of the N-BPs as potential destabilisers through repulsive electrostatic interactions with the positively charged arginine residues of RALA, it is proposed that the side chain groups allows for additional intramolecular ionic interactions between the BPs partially coordinated to the RALA peptide, thus decreasing the number of total arginine side chains required for charge neutralisation. As such, in the case of etidronate, twice as much RALA was required for nano-sized condensation compared to the N-BPs. Nanoparticles formed with each BP and at a mass ratio of 10 conferred a positive zeta potential of greater than 10 mV, supporting the counter-ion condensation theory[20]. Nanoparticle size depends on the polycation, and it is clear that arginine-rich RALA carries out its role as an effective condensing agent[21]. Particle size is critical in terms of uptake into a cell. Although the process is dependent upon the cell type, it has been shown that nanoparticles less than 200 nm undergo spontaneous endocytosis, and as such are optimal for tumour cell uptake[21]. Indeed, it was interesting to note that MDA-MB-231s seemed to internalize FITC-RALA/BP nanoparticles more rapidly than PC3s (Fig. 5).

The positive zeta potential of the nanoparticles facilitates close contact of the nanoparticles with the target cell due to the presence of negatively charged proteoglycans on the cell surface[22]. Non-specific electrostatic interactions between the positively charged nanoparticles and the slight negative charge of the cell can result in uptake into endosomes. Studies in macrophages and osteoclasts have

demonstrated that bone-bound BPs are taken up into these cells by fluid-phase endocytosis, resulting in containment in membrane-bound vesicles[23]. This form of uptake requires acidification of the vesicle to allow neutralisation of the phosphonate head groups, and facilitates diffusion or active transport across the endosomal membrane. Uptake into the cell by this method results in a large fraction of the BP becoming trapped in these intracellular vesicles, meaning only a small proportion is available to exert an effect in the cytosol. This significantly reduces the bioavailability of the BPs. As a consequence, the cytosolic bioavailability of the BPs in skeletal cell lines has not yet been optimised and remains difficult to explain for the bisphosphonates that are active against non-skeletal cancer cell lines, if intracellular enzymes are their sole biological targets. Fortunately, the effects of the BPs, in particular as inhibitors of FPPS, are still substantial so only a small amount needs to escape from the endosome[11].

In contrast, RALA is extremely efficient in escaping the endosome[15]. Indeed the ^{31}P-NMR revealed that at a pH of 4, indicative of the endosome, the particles dissociate and the BP is released. Therefore the BPs clearly remain in solution, even at an acidic pH. Previous studies have shown that at a lower pH the hydrophobic and hydrophilic residues of RALA align, facilitating interactions with the endosome thus releasing the cargo[15]. At cytosolic pH, and in presence of other anionic species entering in competition with the BP for arginine binding, it is likely that the BPs' interactions with RALA decrease thus increasing the concentration of free BP in this organelle, where FFPS, the BPs' biological target, is thought to be present[1]. This clearly supports our theory that RALA acts as a versatile delivery vehicle to carry

charged anionic species across intracellular membranes and release its cargo as the pH changes.

With PC3 cells, neither risedronate nor etidronate, delivered as free drug, were capable of inducing growth inhibition; however, both showed good potency when delivered using RALA. These results confirm that these two bisphosphonates do not modulate extracellular biological targets relevant to cell survival in PC3, although further studies are required to confirm this. The present study also demonstrates that for these two BPs, facilitating intracellularisation re-establishes these BPs as anti-proliferative agents, and this in par with their ability to inhibit key cytosolic enzymatic processes[24]. We have not determined the efficiency of BP encapsulation by RALA. When used to complex nucleic acids, RALA proved to be highly efficient, encapsulating more than 92% of the available pDNA[15]. In the cases of alendronate, and particularly zoledronate, it is conceivable that free BP could partially contribute to the cytotoxicity observed. However, given the lack of cytotoxic potency of etidronate and risedronate, we can confidently conclude that encapsulation with RALA affords the BPs their cytotoxic potency. Therefore, this study suggests that delivery of the BP to the cytosolic compartment results in potent anti-cancer effects, an entirely different mechanism of action and altered pharmacological profile for these two BPs, which requires further elucidation.

There is mounting evidence that some of the observed zoledronate pharmacological effects could be linked to cell surface receptors, including CD73[25]. It is most likely that this is facilitated through an alternative mechanism of cellular entry, as we have previously demonstrated that RALA/DNA nanoparticles predominantly enter

cells via clathrin-mediated endocytosis[15] Future studies could be designed to elucidate whether intracellular delivery of zoledronate that bypasses the CD73 receptor opens up an avenue of therapeutic efficacy to those cells previously resistant to zoledronate induced cell death. Finally, it is also important to note that in order to target tumour cells and spare normal tissue, a targeting peptide could be added on the N-terminus of RALA, designed in a way to recognise overexpressed receptors.

Translation of *in vitro* findings into the *in vivo* setting is a frequent stumbling block. In these initial studies, we injected RALA/alendronate directly into the tumour as proof of principle that the enhanced potency could be translated. Ideally, the RALA/alendronate would be delivered systemically, and studies are ongoing to achieve this.

The observed *in vivo* growth delay is highly significant, as we propose that formulating the BP with RALA alters the BP from a bone specific anti-resorptive drug to an anti-tumour agent. Indeed it is likely that complexation with RALA masks the bone mineral affinity of alendronate; ^{31}P NMR analysis of RALA/alendronate mixed with 0.1 mg/ml hydroxyapatite (HA) produced a spectrum similar to that produced with RALA/alendronate alone, while a second peak was evident on the spectrum when ^{31}P NMR was used similarly for free alendronate mixed with HA (Supplementary Figure 2). This indicates an interaction between free alendronate and HA that was not evident when alendronate was complexed with RALA. It is possible that once the BP has escaped the tumour environment, it no longer exerts an anti-tumour effect, and could revert to its bone resorptive activity, therefore an

optimised dosing regimen is necessary. Furthermore, the dose of BP required to provoke a therapeutic effect would be much lower in the RALA system to achieve anti-resorptive effects, thus potentially negating the limiting side effects of jaw necrosis associated with zoledronate. Fortunately, such dose-limiting side-effects are not associated with alendronate, so it is ideally placed as a candidate BP for further evaluation, development and repurposing, utilising RALA.

Another argument towards the potential of the RALA system in modulating the pharmacological profile of bisphosphonates lies in the fact that many BP-containing compounds have been synthesised and shown extremely promising inhibitory properties against FPPS and GGPS enzymes for instance, but had very poor anti-proliferative activity when evaluated against cell lines. The RALA system offers completely new pharmacological opportunities for this now well established large class of compounds, for which only a few have found a therapeutic niche as anti-resorptive agents.

Acknowledgments

ASM was funded by the Royal Pharmaceutical Society of Great Britain

RC was funded by the EPSRC EP/H031065/1

Supporting Information:

S1 – The size and charge of all four BPs when complexed with the RALA peptide at a range of mass ratios from 2 – 20. Data demonstrates that from a mass ratio of 4 upwards all NPs were less than 100 nm and were positively charged.

S2 – This 31P NMR confirms that when RALA is present there is no free alendronate present to interact with the HA in this instance. This demonstrates that all of the BP is complexed by RALA.

References

1. Ebetino, F. H.; Hogan, A. M.; Sun, S.; Tsoumpra, M. K.; Duan, X.; Triffitt, J. T.; Kwaasi, A. A.; Dunford, J. E.; Barnett, B. L.; Oppermann, U.; Lundy, M. W.; Boyde, A.; Kashemirov, B. A.; McKenna, C. E.; Russell, R. G. The relationship between the chemistry and biological activity of bisphosphonates. *Bone* **2011**, *49* (1), 20-33.

2. Vassiliou, V.; Kardamakis, D. The management of metastatic bone disease with the combination of bisphosphonates and radiotherapy: From theory to clinical practice*. Anticancer Agents Med Chem.* **2009***, 9* (3), 326-335.

3. Paterson, A.; Powles, T. J.; Kanis, J. A.; McCloskey, E.; Hanson, J.; Ashley, S. Double-blind controlled trial of oral clodronate in patients with bone metastases from breast cancer. *J Clin Oncol.* **1993**, 11 (1), 59-65.

4. Ibrahim, T.; Mercatali, L.; Sacanna, E.; Tesei, A.; Carloni, S.; Ulivi, P.; Liverani, C.; Fabbri, F.; Zanoni, M.; Zoli, W.; Amadori, D. Inhibition of breast cancer cell proliferation in repeated and non-repeated treatment with zoledronic acid. *Cancer Cell Int.* **2012,** 12 (1), 48-60.

5. Mani, J.; Vallo, S.; Barth, K.; Makarević, J.; Juengel, E.; Bartsch, G.; Wiesner, C.; Haferkamp, A.; Blaheta, R. A. Zoledronic acid influences growth, migration and invasive activity of prostate cancer cells in vitro. *Prostate Cancer Prostatic Dis.* **2012,** 15 (3), 250-255.

6. Metcalf, S.; Pandha, H. S.; Morgan, R. Antiangiogenic effects of zoledronate on cancer neovasculature. *Future Oncology* **2011,** 7 (11), 1325-1333.

7. Ottewell, P. D.; Lefley, D. V.; Cross, S. S.; Evans, C. A.; Coleman, R. E.; Holen, I. Sustained inhibition of tumor growth and prolonged survival following sequential administration of doxorubicin and zoledronic acid in a breast cancer model. *Int. J. Cancer* **2010**, 126 (2), 522-532.

8. Daubiné, F.; Le Gall, C.; Gasser, J.; Green, J.; Clézardin, P. Antitumor effects of clinical dosing regimens of bisphosphonates in experimental breast cancer bone metastasis. *J. Natl. Cancer Inst.* **2007,** 99 (4), 322-330.

9. Hiraga, T.; Williams, P. J.; Ueda, A.; Tamura, D.; Yoneda, T. Zoledronic acid inhibits visceral metastases in the 4T1/luc mouse breast cancer model. *Clin. Cancer Res.* **2004**, 10(13), 4559-4567.

10. Aft, R.; Perez, J.; Raje, N.; Hirsh, V.; Saad, F. Could targeting bone delay cancer progression? potential mechanisms of action of bisphosphonates. *Crit. Rev. Oncol.* **2012**, 82 (2), 233-248.

11. Zhang, Y.; Cao, R.; Yin, F.; Hudock, M. P.; Guo, R. T.; Krysiak, K.; Mukherjee, S.; Gao, Y. G.; Robinson, H.; Song, Y.; No, J. H.; Bergan, K.; Leon, A.; Cass, L.; Goddard, A.; Chang T, K.; Lin, F. Y.; Van Beek, E.; Papapoulos, S.; Wang, A. H.; Kubo, T.; Ochi, M.; Mukkamala, D.; Oldfield, E. Lipophilic bisphosphonates as dual farnesyl/geranylgeranyl diphosphate synthase inhibitors: an X-ray and NMR investigation. *J. Am. Chem. Soc.* **2009**, 131 (14), 5153-62.

12. Chebbi, I.; Migianu-Griffoni, E.; Sainte-Catherine, O.; Lecouvey, M.; Seksek, O.; (2010) In vitro assessment of liposomal neridronate on MDA-MB-231 human breast cancer cells. *Int. J. Pharm.* **2010**, 383 (1), 116-122.

13. Marra, M.; Salzano, G.; Leonetti, C.; Tassone, P.; Scarsella, M.; Zappavigna, S.; Calimeri, T.; Franco, R.; Liguori, G.; Cigliana, G.; Ascani, R.; La Rotonda, M. I.; Abbruzzese, A.; Tagliaferri, P.; Caraglia, M.; De Rosa, G. Nanotechnologies to use bisphosphonates as potent anticancer agents: The effects of zoledronic acid encapsulated into liposomes. *Nanomedicine: Nanotechnology, Biology and Medicine* **2011**, 7 (6), 955-964.

14. Salzano, G.; Marra, M.; Porru, M.; Zappavigna, S.; Abbruzzese, A.; La Rotonda, M. I.; Leonetti, C.; Caraglia, M.; De Rosa, G. Self-assembly nanoparticles for the delivery of bisphosphonates into tumors. *Int. J. Pharm.* **2011**, 403 (1), 292-297.

15. McCarthy, H. O.; McCaffrey, J.; McCrudden, C. M.; Zholobenko, A.; Ali, A. A.; McBride, J. W.; Massey, A. S.; Pentlavalli, S.; Chen, K. H.; Cole, G.; Loughran, S. P.; Dunne, N. J.; Donnelly, R. F.; Kett, V. L.; Robson, T. Development and characterization of self-assembling nanoparticles using a bio-inspired amphipathic peptide for gene delivery. *J. Control Rel.* **2014**, 189: 141-149.

16. Banerjee, A.; Raad, F. S.; Vankova, N.; Bassil, B. S.; Thomas Heine, T.; Kortz, U. Polyoxomolybdodiphosphonates: Examples incorporation ethylidenepyridines. *Inorg. Chem*. **2011**, 50 (22), 11667 – 11675.

17. Singh, S. K.; Manne, N.; Ray, P. C.; Pal, M. Synthesis of imidazol-1-yl-acetic acid hydrochloride: A key intermediate for Zoledronic acid. *Beilstein J. Org. Chem.* **2008**, 4, 42 .

18. Milen, M.; Grün, A.; Bálint, E.; Dancsó, A.; Keglevich, G. Solid–Liquid Phase Alkylation of *N*-Heterocycles: Microwave-Assisted Synthesis as an Environmentally Friendly Alternative. *Synth. Commun.* **2010**, 40(15), 2291-2301.

19. Rubino, M. T.; Agamennone, M.; Campestre, C.; Campiglia, P.; Cremasco, V.; Faccio, R.; Laghezza, A.; Loiodice, F.; Maggi, D.; Panza, E.; Rossello, A.; Tortorella, P. Biphenyl Sulfonylamino Methyl Bisphosphonic Acids as Inhibitors of Matrix Metalloproteinases and Bone Resorption. *Chem. Med. Chem.* **2011**, 6(7), 1258–1268.

20. Bagwe, R. P.; Hilliard, L. R.; Tan, W. Surface modification of silica nanoparticles to reduce aggregation and nonspecific binding. *Langmuir* **2006***,* 22(9), 4357-4362.

21. He, C.; Hu, Y.; Yin, L.; Tang, C.; Yin, C.; Effects of particle size and surface charge on cellular uptake and biodistribution of polymeric nanoparticles*. Biomaterials* **2010**, 31(13), 3657-3666.

22. Konate, K.; Crombez, L.; Deshayes, S.; Decaffmeyer, M.; Thomas, A.; Brasseur, R.; Aldrian, G.; Heitz, F.; Divita, G. Insight into the cellular uptake mechanism of a secondary amphipathic cell-penetrating peptide for siRNA delivery*. Biochem.* **2010**, 49 (16), 3393-3402.

23. Thompson, K.; Rogers, M. J.; Coxon, F. P.; Crockett, J.C. Cytosolic entry of bisphosphonate drugs requires acidification of vesicles after fluid-phase endocytosis*. Mol. Pharmacol.* (2006) 69(5), 1624-1632.

24. Kavanagh, K. L.; Guo, K.; Dunford, J. E.; Wu, X.; Knapp, S.; Ebetino, F. H.; Rogers, M. J.; Russell, R. G.; Oppermann, U.The molecular mechanism of nitrogen-containing bisphosphonates as antiosteoporosis drugs*. PNAS* **2006,** 103(20), 7829-7834.

25. Rodríguez-Lozano, F.J.; García-Bernal, D.; Ros-Roca Mde, L.; Algueró Mdel, C.; Oñate-Sánchez, R.E.; Camacho-Alonso, F.; Moraleda, J.M. Cytoprotective effects of melatonin on zoledronic acid-treated human mesenchymal stem cells in vitro. *J Craniomaxillofac Surg* **2015**, 43(6), 855-62.

Table 1: Formulation and molar ratio of RALA/BP NPs for a 10:1 formulation

Bisphosphonate	Molecular weight (g/mol)	Moles BP in 1 μg	Moles RALA in 10 μg	Mole Ratio RALA: BP
Etidronate	206.1	4.85×10^{-9}	3×10^{-8}	16.1
Alendronate	249.1	4.01×10^{-9}	3×10^{-8}	13.4
Zoledronate	272.1	3.68×10^{-9}	3×10^{-8}	12.2
Risedronate	283.1	3.53×10^{-9}	3×10^{-8}	11.7

Table 2: Summary of physiochemical characteristics of the RALA/BP NPs

Bisphosphonate	Average Size Range	Mole:Mole ratio at the lowest mass ratio formulation	Zeta Potential at 10:1 RALA/BP	Poly Dispersity Index at 10:1 RALA/BP	Particle count at 10:1 RALA/BP (Kcps)
Etidronate	>4:1 mass ratio 40-70 nm	0.40	15.3	0.478	104
Alendronate	>2:1 mass ratio 40-60 nm	0.66	17	0.536	74
Zoledronate	>2:1 mass ratio 40-60 nm	0.61	11.45	0.494	109
Risedronate	>2:1 mass ratio 30-60 nm	0.58	17.6	0.490	122

Table 3: The potentiation conferred by RALA delivery of the BPs

			EC_{50} (μM) (95% confidence intervals)		Potentiation factor
			BP alone	RALA/BP	
MTS assay	MDA-MB-231	Alendronate	166 (128 – 192)	29 (20 – 61.9)	5.7
		Zoledronate	86.3 (73.3 – 101.6)	25.7 (17.3 – 36.3)	3.4
	PC3	Alendronate	147 (125.2 – 172.8)	35.7 (19.7 – 64.6)	4.1
		Zoledronate	56.3 (41.3 – 76.8)	39.3 (26.5 – 58.3)	1.4
Blue exclusion	MDA-MB-231	Alendronate	119 (94.1 –	70 (46.9 –	1.7

			149.1)	104.5)	
		Zoledronate	88.3 (70.8 – 110.2)	37.9 (25.7 – 56.1)	2.3
	PC3	Alendronate	106.4 (99.6 – 113.7)	18.4 (16.1 – 21.0)	5.8
		Zoledronate	28.5 (24.5 – 33.0)	26.3 (25.0 – 27.7)	1.08
		Etidronate	N/A	31.7 (25.0 – 40.4)	N/A
		Risedronate	N/A	32.1 (26.2 – 39.2)	N/A

Figure 1

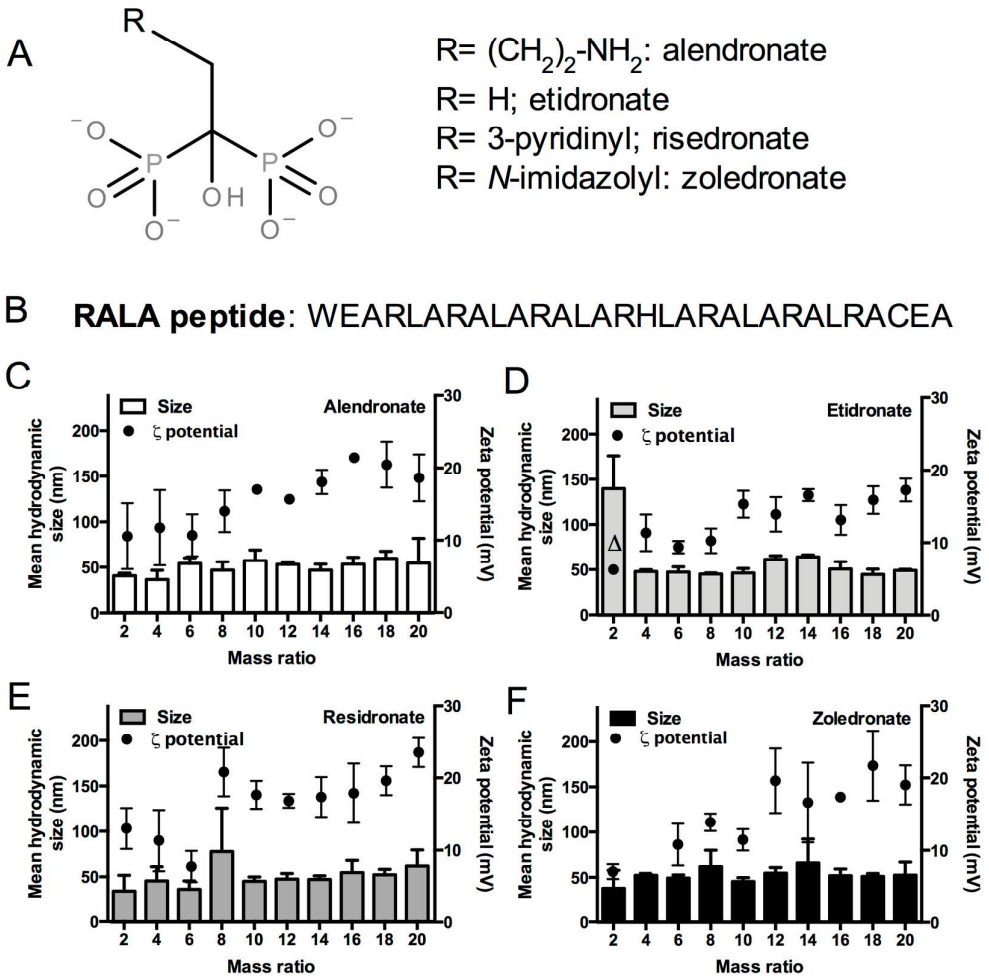

Figure 1. A: Structure of the bisphosphonates employed in the study. **B:** The RALA sequence. Mean hydrodynamic size and zeta potential of **C:** RALA/alendronate nanoparticles, **D:** RALA/etidronate nanoparticles, **E:** RALA/risedronate nanoparticles and **F:** RALA/zoledronate nanoparticles (Bars/points represent mean ± SEM; N=3). Δp< 0.05 compared with zeta potential at mass ratio 10.

Figure 2

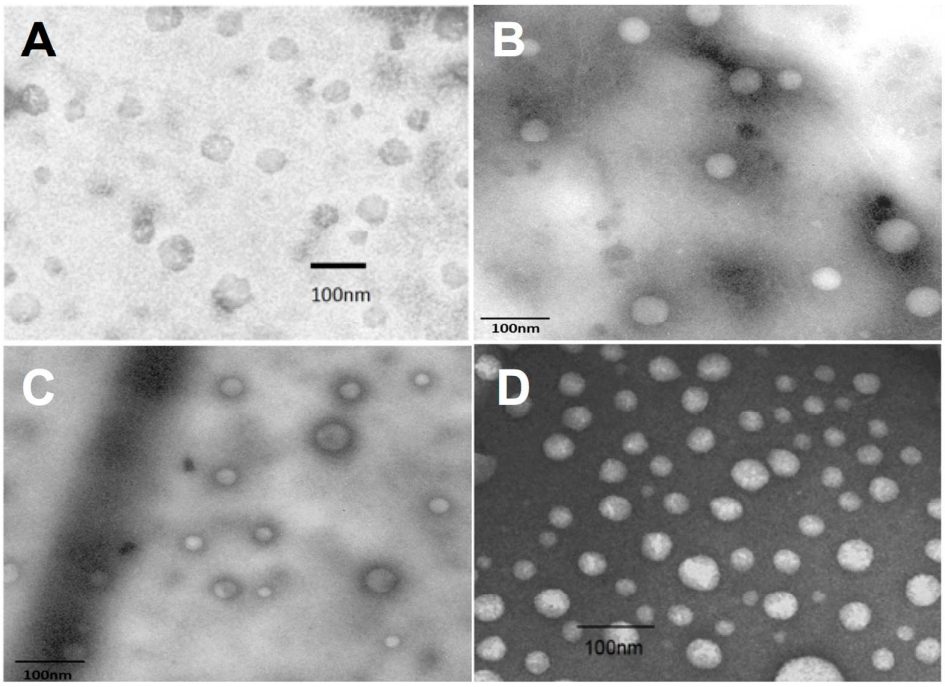

Figure 2. Nanoparticles were prepared at a mass ratio of 10:1 and allowed to incubate for 30 min before being loaded onto carbon reinforced formvar coated copper grids. Samples were stained with 5% uranyl acetate. Nanoparticles were imaged using a JEOL 100CXII transmission electron microscope. **A:** RALA/alendronate nanoparticles; **B:** RALA/etidronate nanoparticles; **C:** RALA/risedronate nanoparticles; **D:** RALA/zoledronate nanoparticles.

Figure 3

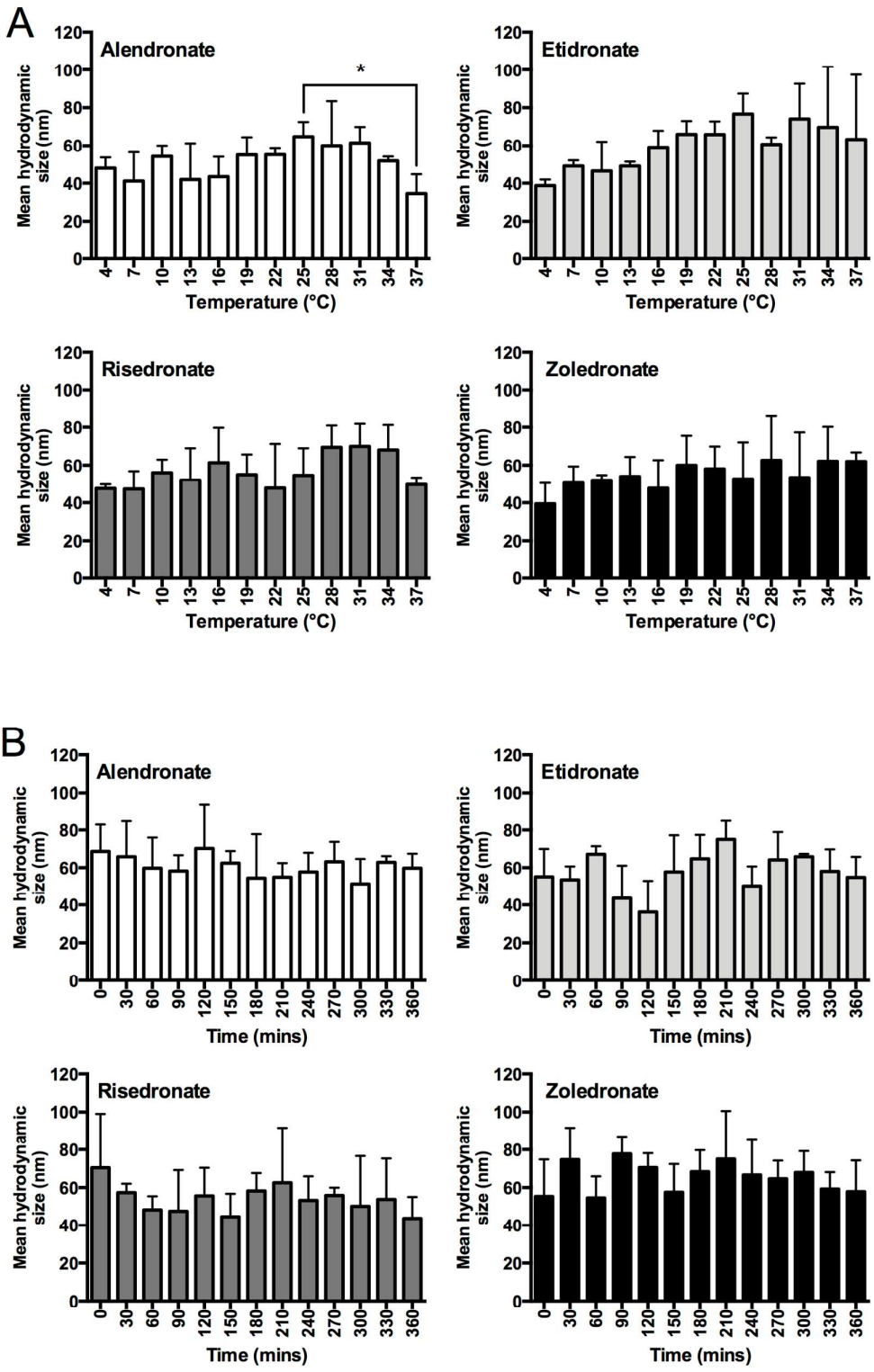
A
Alendronate
Etidronate
Risedronate
Zoledronate
Mean hydrodynamic size (nm)
Temperature (°C)
*
B
Alendronate
Etidronate
Risedronate
Zoledronate
Mean hydrodynamic size (nm)
Time (mins)

Figure 3. A: Mean hydrodynamic size of RALA/BP nanoparticles was determined to assess thermal stability over a range of temperatures. **B:** Mean hydrodynamic size of RALA/BP nanoparticles was determined to assess stability across a 6 h time period. Both studies used RALA/BP at a mass ratio of 10:1. (Bars represent mean ± SEM; N=3). * $p < 0.05$.

Figure 4

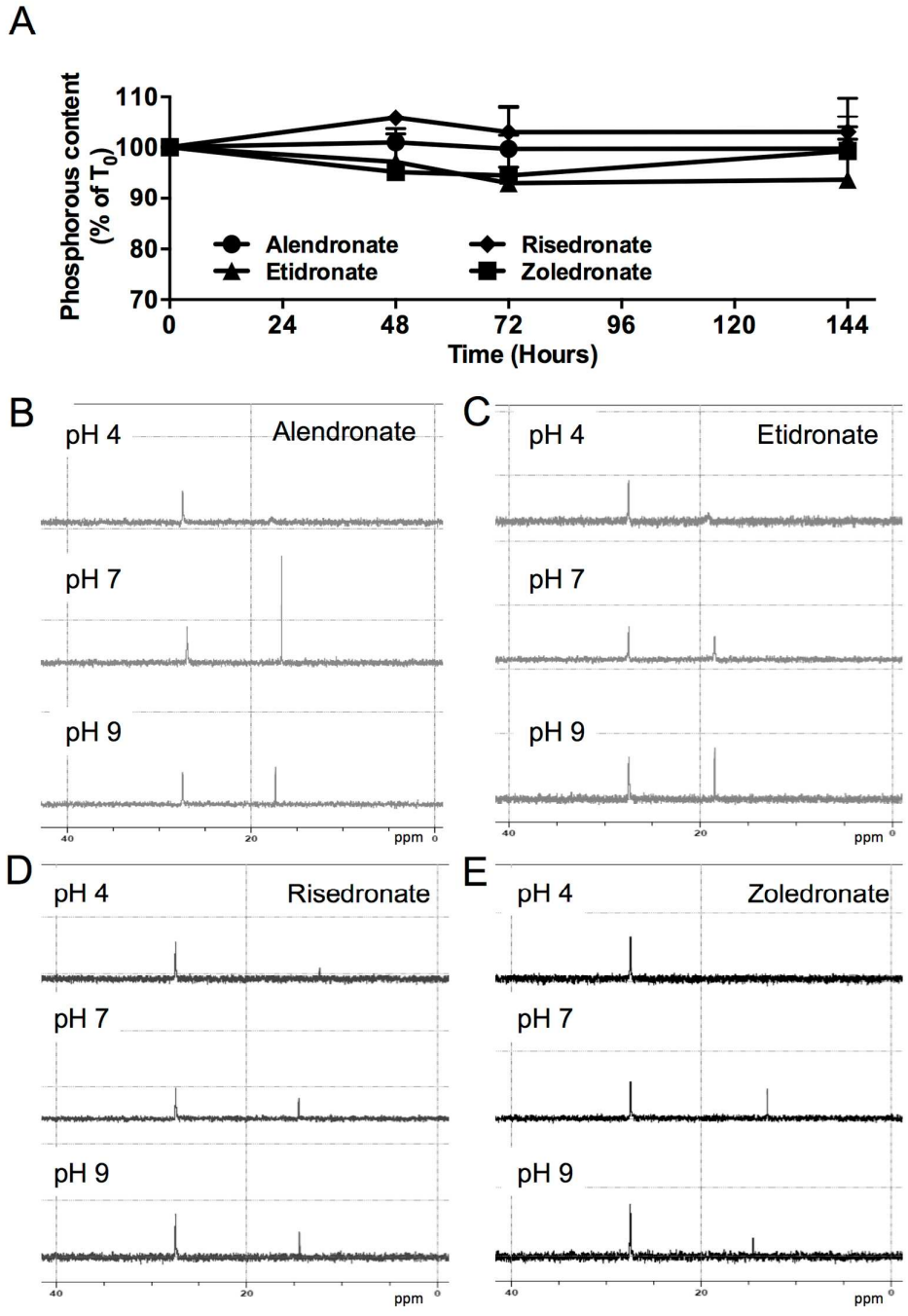

Figure 4. ^{31}P NMR Stability. pH 7.0, RT, 1.0 mM of BP. **A:** RALA/BP nanoparticles were prepared at a mass ratio of 10:1. Phosphorous NMR was used to detect the presence of BP in the sample using internal standard trimethyl phosphate (1.0 mM).

These samples were analysed at regular time intervals over a period of one week. **B:** All nanoparticles were prepared at a mass ratio of 10:1. ^{31}P-NMR was used to analyse 500 µl aliquots at pH 4, 7 and 9, referenced to a HMPA probe and were performed immediately after pH adjustment by the dropwise addition of either 0.1 M HCl or 0.1 M NaOH. **B:** RALA/alendronate; **C:** RALA/etidronate; **D:** RALA/risendronate; **E:** RALA/zoledronate.

Figure 5

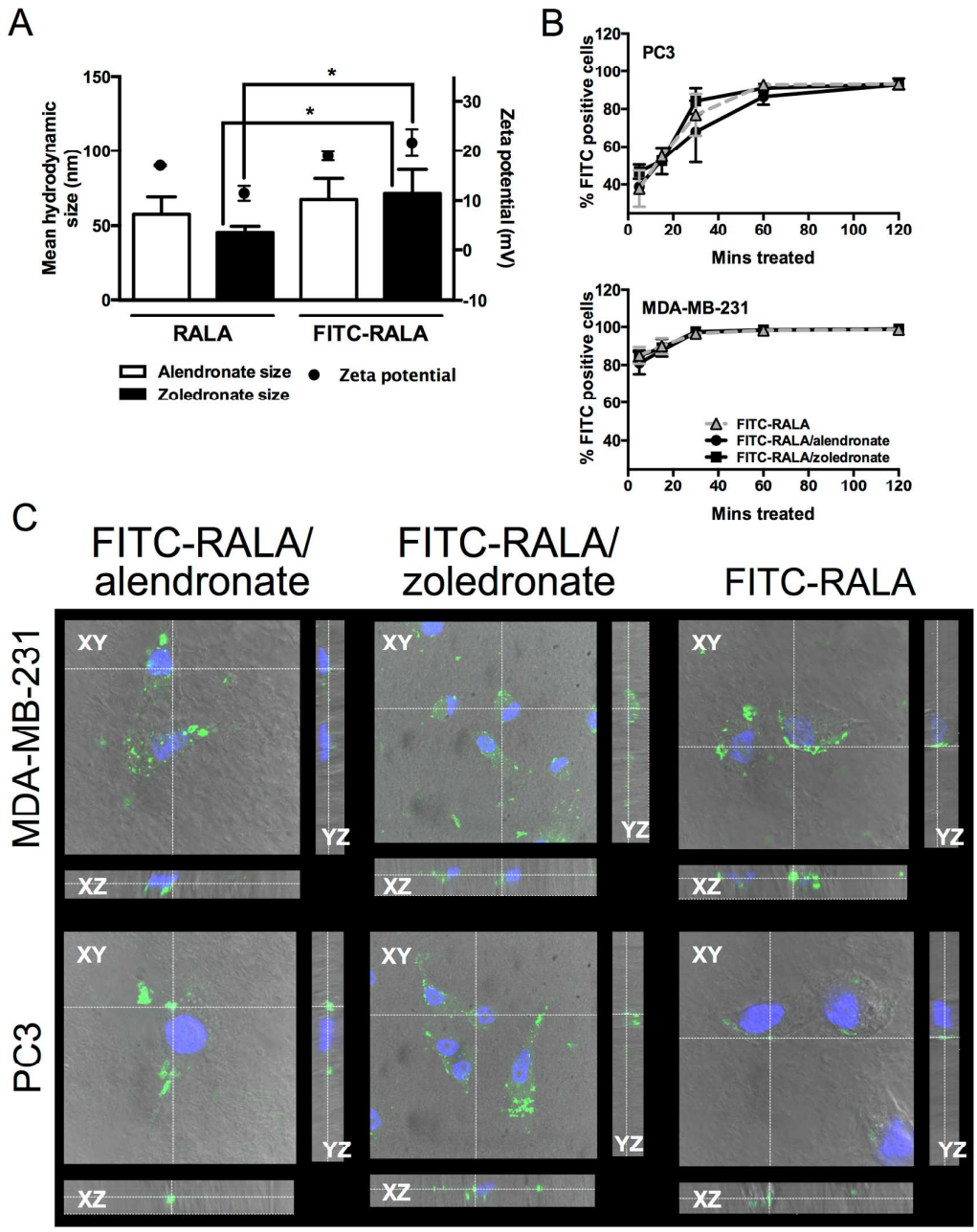

Figure 5. Internalization of FITC-RALA/BP nanoparticles in PC3 and MDA-MB-231. A: Size and charge of particles complexed using FITC-RALA with alendronate and zoledronate; B: analysis of nanoparticle internalization by flow cytometry analysis of

FITC content; C: confocal fluorescence microscopy of FITC localization, with orthogonal sectioning.

Figure 6

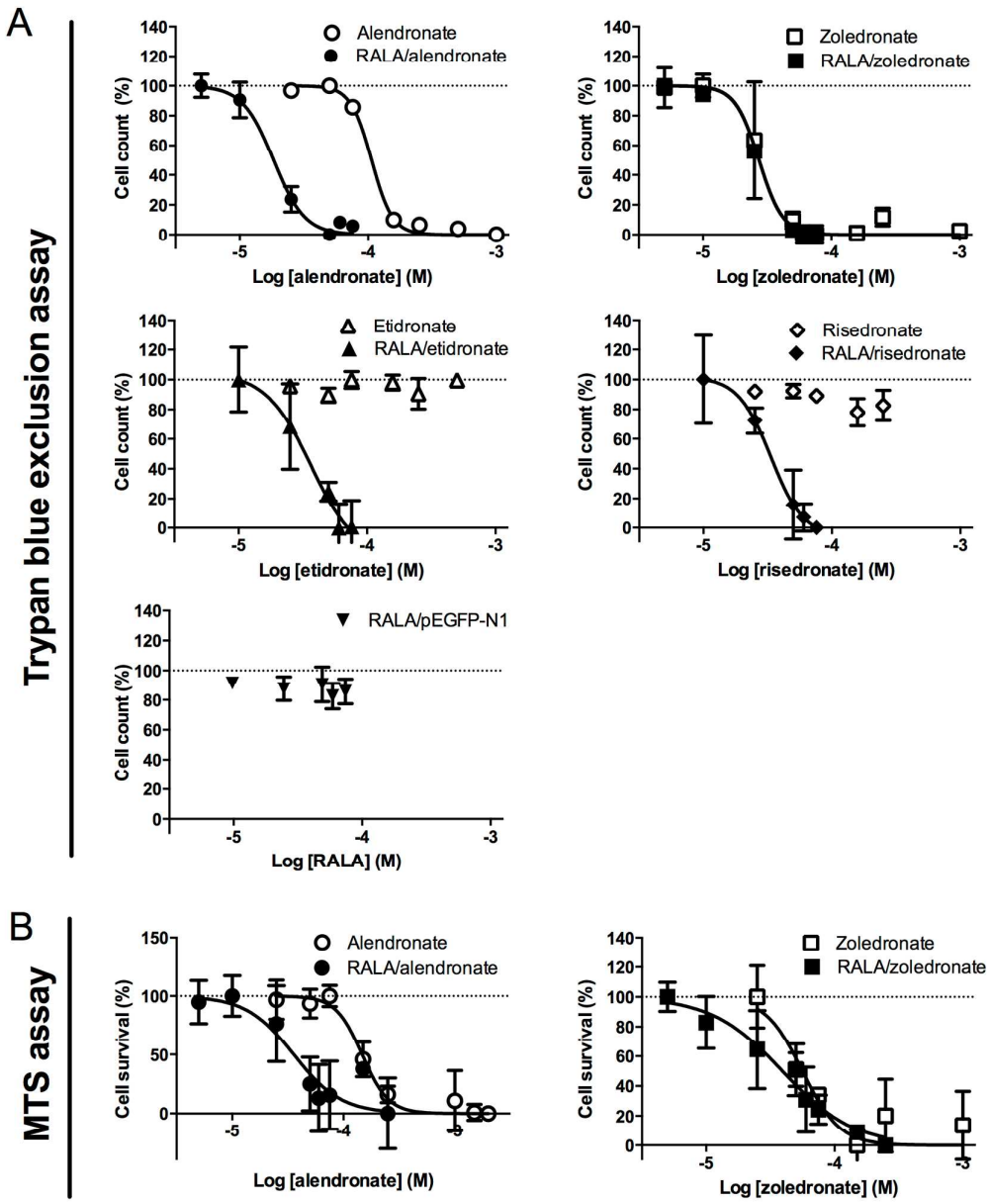
A
Trypan blue exclusion assay
Alendronate
RALA/alendronate
Cell count (%)
Log [alendronate] (M)
Zoledronate
RALA/zoledronate
Log [zoledronate] (M)
Etidronate
RALA/etidronate
Log [etidronate] (M)
Risedronate
RALA/risedronate
Log [risedronate] (M)
RALA/pEGFP-N1
Log [RALA] (M)
B
MTS assay
Cell survival (%)
Alendronate
RALA/alendronate
Log [alendronate] (M)
Zoledronate
RALA/zoledronate
Log [zoledronate] (M)

Figure 6. Assessment of the impact of free- and RALA-complexed BPs (alendronate, etidronate, residronate and zoledronate) on the viability of PC3 prostate cancer cells. Cell viability was assessed by Trypan Blue exclusion assay (A) and MTS cell viability assay (B). When a dose-response relationship existed, non-linear regression analysis was performed and EC_{50}s calculated (presented next to their respective curves; N/A – no IC_{50} as no dose-response relationship existed). The impact of RALA/pEGFP-N1 nanoparticles on viability was assessed to control for general toxicity of RALA nanoparticles.

Figure 7

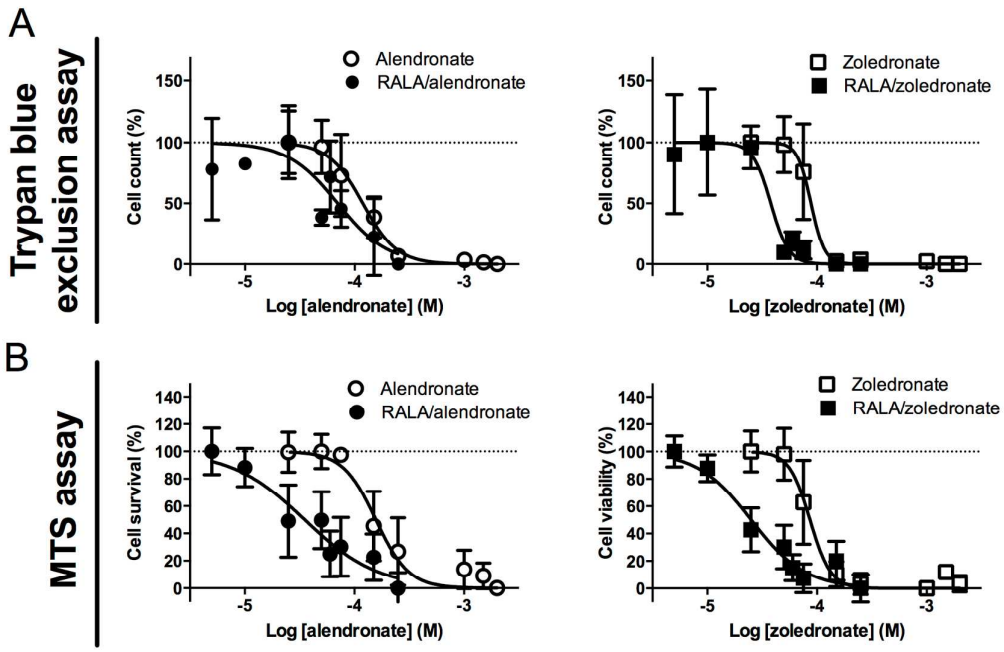

Figure 7. Assessment of the impact of free- and RALA-complexed BPs (alendronate and zoledronate) on the viability of MDA-MB-231 breast cancer cells. Cell viability was assessed by Trypan Blue exclusion assay (A) and MTS cell viability assay (B). When a dose-response relationship existed, non-linear regression analysis was performed and EC_{50}s calculated (presented next to their respective curves).

Figure 8

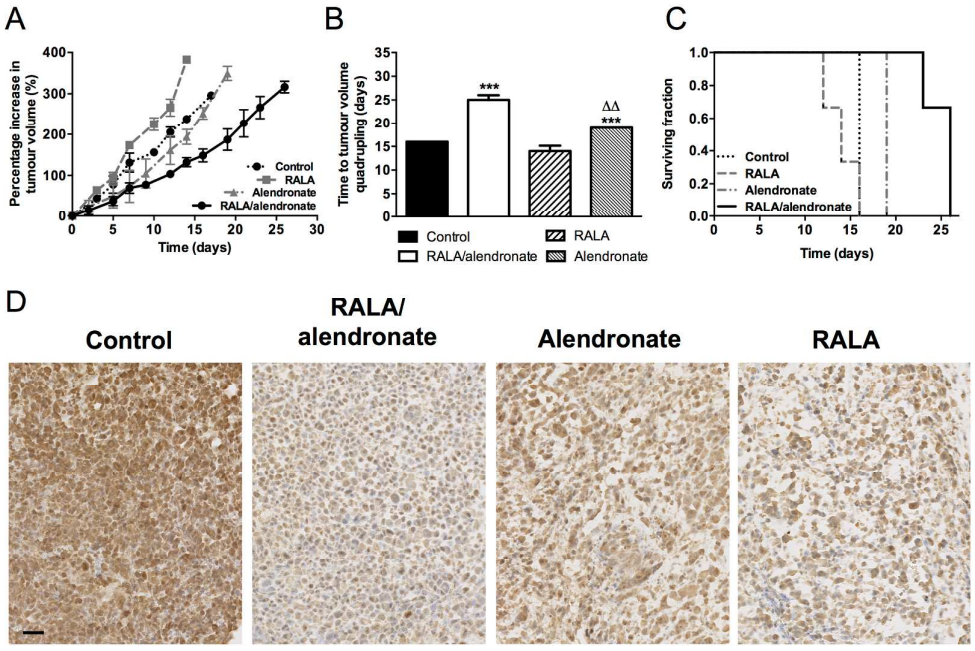

Figure 8. PC3 prostate cancer cell xenografts were implanted on the rear dorsum of BALB-c SCID mice and grown until the volume reached approximately 100 mm^3. Treatments were thrice weekly for three weeks via intratumoural injection with mice being assigned randomly to either an untreated, RALA only, free alendronate or RALA/alendronate treatment group (N=3). The experimental endpoint was quadrupling of tumour volume. **A:** Percentage increase in tumour volume. **B:** Time taken for tumour growth to quadruple. ***$p<0.001$ compared with control; $^{\Delta\Delta}p<0.01$ compared with RALA/alendronate. **C:** Kaplan-Meier survival plot. Censoring was not required. **D:** Immunohistochemical analysis of Ki67 expression in control and RALA/alendronate-treated mice. Representative regions of sections are displayed. Scale represents 50 µm.

Table of Contents/Abstract Graphic

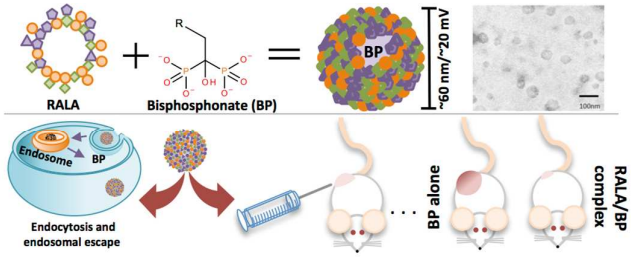

Bisphosphonates are condensed into nanoparticles via the RALA peptide. The intracellular delivery of these RALA/BP nanoparticles significantly enhances the anti-cancer effects *in vitro* and *in vivo*.